Article

Experimental Analysis on the Influence of Operating Profiles on High Temperature Polymer Electrolyte Membrane Fuel Cells

Tancredi Chinese [1], Federico Ustolin [2,3], Benedetta Marmiroli [4], Heinz Amenitsch [4] and Rodolfo Taccani [2,*]

1   Cenergy srl, c/o AREA Science Park, Basovizza, 34149 Trieste, Italy; tancredi.chinese@cenergy.it
2   Dipartimento di Ingegneria e Architettura, Università degli studi di Trieste, Via Valerio 10, 34127 Trieste, Italy
3   Department of Mechanical and Industrial Engineering, Norwegian University of Science and Technology NTNU, Richard Birkelands vei 2B, 7034 Trondheim, Norway; federico.ustolin@ntnu.no
4   Institute of Inorganic Chemistry, Graz University of Technology, Stremayrgasse 9/IV, 8042 Graz, Austria; benedetta.marmiroli@elettra.eu (B.M.); heinz.amenitsch@elettra.eu (H.A.)
*   Correspondence: taccani@units.it

Abstract: The Energy System lab at the University of Trieste has carried out a study to investigate the reduction in performance of high temperature polymer electrolyte membrane (HTPEM) fuel cell membrane electrode assemblies (MEAs) when subjected to different ageing tests. In this study, start and stop cycles, load cycles, open circuit voltage (OCV) permanence and constant load profile were considered. Polarization curves (PC) together with electrochemical impedance spectroscopy (EIS) and cyclic voltammetry (CV) data were recorded during the ageing tests to assess the fuel cell performance. In this paper, experimental data are presented to confirm the test methodology previously proposed by the authors and to quantitatively correlate the performance degradation to the operational profiles. It was demonstrated that OCV condition, start and stop and load cycling increase degradation of the MEAs with respect to constant load operation. As expected, the OCV is the operational condition that influences performance degradation the most. Finally, the MEAs were analyzed with synchrotron small angle X-ray scattering (SAXS) technique at the Austrian SAXS beamline at Elettra-Sincrotrone Trieste to analyze the nano-morphological catalyst evolution. As for the catalyst morphology evolution, the ex situ SAXS methodology proposed by the authors is confirmed in its ability to assess the catalyst nanoparticles aggregation.

Keywords: hydrogen; fuel cell; high temperature polymer electrolyte membrane; membrane electrode assembly; operating profiles; performance degradation; electrochemical surface area; polarization curve; SAXS analysis

1. Introduction

Polybenzimidazole (PBI)-based high temperature polymer electrolyte membrane (HTPEM) fuel cells are a suitable alternative to Nafion-based low temperature PEM (LTPEM), especially for micro–combined heat and power (mCHP) applications. Nevertheless, high costs and degradation are still two major issues to be overcame to achieve commercialization [1,2]. The high cost is greatly influenced by the platinum-based electrocatalysts needed to facilitate the kinetics of the electrode reactions. The catalyst is made by platinum (Pt) or Pt alloy nanoparticles (NPs) on a porous carbon support to increase the electrochemical surface area (ECSA). Degradation of the catalyst layer may induce processes which are responsible for the performance losses of the membrane electrode assembly (MEA) when subjected to fuel cell operational conditions [3,4]. Furthermore, the modification of the phosphoric acid position and content in the PBI membrane and thinning of this latter can deteriorate the MEA performance [5,6]. It has been speculated that Ostwald ripening [7] and coalescence [8] mechanisms can provoke the degradation of the catalyst layer by reducing the ECSA [9]. This loss is affected by particle size: the smaller the

particle, the greater the tendency for its coarsening. Therefore, the reduction of the expensive Pt loading by minimizing catalyst particle size, and hence increasing the ECSA/weight Pt ratio, have the major drawback to increase the ECSA loss rate [10]. The improvement of the PEM fuel cell efficiency and durability can be obtained by investigating the physical processes that lead to the agglomeration of the catalyst particles. Several studies show the dependence of the catalyst agglomeration on the operating conditions [11].

High potentials are responsible of the degradation of the catalyst and its support [12]. The Pt particle agglomeration is increased by open circuit voltage (OCV) because both Pt oxidation and carbon corrosion are favoured at high electrode potential (approx. at 1 V [13]). The Pt oxidation initiates the dissolution and the Ostwald ripening process [14]. On the other hand, the carbon corrosion triggers the agglomeration by coalescence [14]. Then, the carbon corrosion can lead to platinum detachment [15]. In [16], a 1200 h test was carried out with a six-cell PEM fuel cell (PEMFC) stack operating close to OCV. A significant reduction of the PEMFC stack performance was observed after 800 h. Catalyst degradation was assumed to be the cause of cell deterioration in the first part of the experiment, while membrane failure probably led to the subsequent decay. In [15], the impact of OCV on the performance of HT-PEMFCs was investigated. In particular, the procedure consisted of a rapid OCV increment during the first few minutes and a slower increase until a peak after 35 min. Electrochemical impedance spectroscopy (EIS) indicated loss of catalyst activity and X-ray diffraction (XRD) showed an increase of 430% of the cathode Pt crystallites size after 244.5 h of OCV exposure. In [17], a similar result was reported during a 250 h ageing test under OCV condition.

To better understand the degradation phenomena involved in PEM fuel cells, several diagnostic tools such as polarization curve (PC), electrochemical impedance spectroscopy (EIS) and cyclic voltammetry (CV) have been used by different authors. Among nano-morphological analysis techniques, small angle X-ray scattering (SAXS) can support the study of catalyst degradation. SAXS is a method to characterize the MEA of a fuel cell and its degradation. This technique can provide information about size, shape and distribution of catalyst nano-particles over large portion of the active area both in situ and ex situ [3,10]. The use of this technique to investigate growth and transformations of carbon-supported Pt nanoparticle electrocatalysts was pioneered by Haubold et al. [18]. Later, Stevens et al. [19] exploited ex-situ SAXS to determine Pt particle size distribution. Yu et al. [20] carried out an in-situ SAXS analysis that allowed time-resolved study of Pt particle growth under potential cycling. In [10], SAXS is used to examine, in situ, a carbon-supported PEM cathode electrocatalyst. The authors analyzed the growth of Pt particles due to potential load cycles for two different Pt catalyst loads: 20%wt and 40%wt. They observed that particle size increased rapidly over the first 8 h for 20-Pt while a slower growth was reached at ~3.2 nm. Contrarily, 40-Pt with an initial particle size of 3.2 nm, exhibited a steady particle growth from the beginning of the test. In [21], an analysis was carried out of Pt agglomeration through *operando* anomalous small angle X-ray scattering (ASAXS) on a catalyst subjected to different load cycling in a MEA environment and in aqueous environment. This analysis showed that for all tests there was a loss of particles with a diameter smaller than 3.0 nm, and an increment of larger particles. In this study, it was demonstrated that Pt nanoparticle surface area loss generated by potential cycling can be limited by lessening the particles tinier than a critical particle diameter (CPD) (3.5 ÷ 4.0 nm). It may be concluded that few morphological analyses of the HTPEM MEAs subjected to different loading cycles were conducted in the past. This study aims to provide additional experimental data to fulfil the current knowledge dearth on this topic.

In this paper, the authors present the most recent advances of a research activity that concerns the analysis of degradation of HTPEM [3,11]. In particular, the effects of open circuit voltage (OCV) and start-stop (SS) cycles are considered. During operation, polarization curves, EIS and CV were conducted. Catalyst nano-morphology evolution was assessed by employing the ex situ SAXS technique. SAXS was performed on six MEAs to complete the degradation analysis started by the authors in previous works where MEAs

were subjected to constant load, triangular loading cycling with and without OCV and start and stop cycles [3,11]. To the authors' knowledge, the SAXS technique was used to analyze HTPEM MEA constantly subjected to OCV for the first time. A new unloaded MEA was also analyzed by means of SAXS technique as reference data.

2. Materials and Methods

The MEAs used in the test are Celtec-P 1000, commercial phosphoric acid (H_3PO_4)/PBI MEAs for high temperature PEM fuel cells produced and distributed by BASF Fuel Cell Company (Ludwigshafen, Germany). The carbon support in the catalyst layer is Vulcan XC-72, the catalyst is Pt-alloy (0.75 mgPt/cm^2) at the cathode and Pt (1 mgPt/cm^2) at the anode. Phosphoric acid doping level is 70PA/repeat unit. During tests all MEAs were operated with hydrogen and air at the anode and cathode, respectively. The schematic of the test bench used for the aging tests is presented in Figure 1. The reactants inlet pressures were measured by means of pressure transducers. The anode and cathode temperatures were measured by using K-type thermocouples installed on the endplates. Two mass flow controllers (Sierra SmartTrack M100 (Sierra, Monterey, CA, USA) and Bronkhorst El-Flow F201 (Bronkhorst, Ruurlo, The Netherlands) for the air and hydrogen circuits, respectively) were employed to measure and set the reactant flow rates.
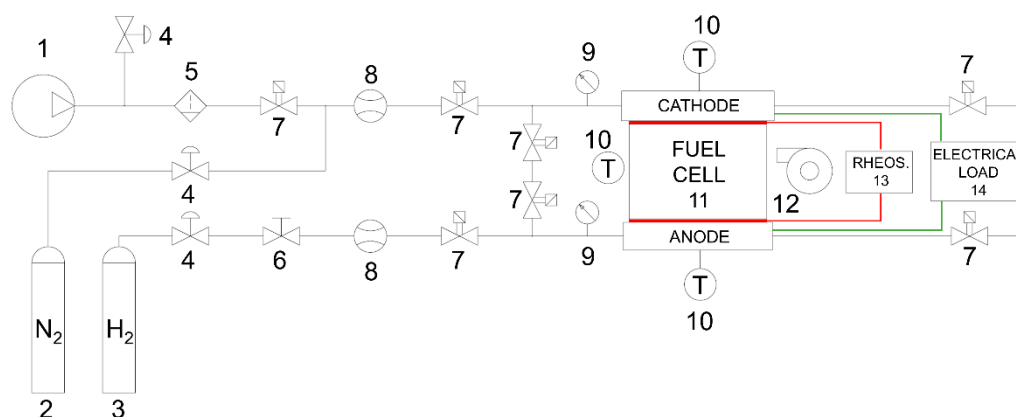

Figure 1. Test bench simplified schematic: (1) air compressor, (2) nitrogen bottle, (3) hydrogen reservoir, (4) pressure regulator valves, (5) air filter, (6) valve, (7) solenoid type valves, (8) flow meters, (9) pressure transducers, (10) thermocouples, (11) fuel cell, (12) air blower, (13) rheostat and (14) electrical load.

With the purpose of comparing the experimental data, all tests were performed following the methodology already adopted by the authors in previous works [3,11]. As suggested by the manufacturer, all MEAs were operated for 100 h under constant conditions (T = 160 °C, i = 0.22 A/cm^2) before starting the degradation tests. Two aging profiles were tested on three MEAs hereafter named MEA OCV_1, MEA SS_2 and MEA OCV_2 and afterwards compared with the results already previously obtained by the authors [3,11] on MEAs named MEA TRG, MEA TRG_OCV_1, MEA SS_1, MEA TRG_OCV_2, MEA CL_1, MEA CL_2 (TRG stays for triangular cycles while CL for constant load). During load cycling, MEAs temperature was held at 160 °C. A constant air flowrate of 2.0 sl/min was set without backpressure at the cathode outlet. The anode was maintained in dead-end operation with a purge every three minutes only during the test cycles.

In Table 1, a description of the load profiles for each MEA tested by authors until now is reported, while these profiles are displayed in Figure 2.

Table 1. Load profiles description of all membrane electrode assemblies (MEAs) (abbreviations: TRG: triangular sweep cycles, OCV: open circuit voltage, CL: constant load, SS: start and stop).

MEA Label	Load Profiles
MEA Ref_1, MEA Ref_2	Unloaded MEA used as reference
MEA TRG	100,000 triangular sweep cycles between open circuit voltage (OCV) and 0.5 A/cm^2 corresponding to 440 h of operation
MEA TRG_OCV_1, MEA TRG_OCV_2	125,000 triangular sweep cycles between OCV and 0.5 A/cm^2 with 2 s of permanence at OCV corresponding to 550 h of operation
MEA CL_1, MEA CL_2	550 h of constant load operation at 0.22 A/cm^2
MEA SS_1 MEA SS_2	1000 start and stop cycles300 start and stop cycles
MEA OCV_1 MEA OCV_2	126 h of constant OCV400 h of constant OCV
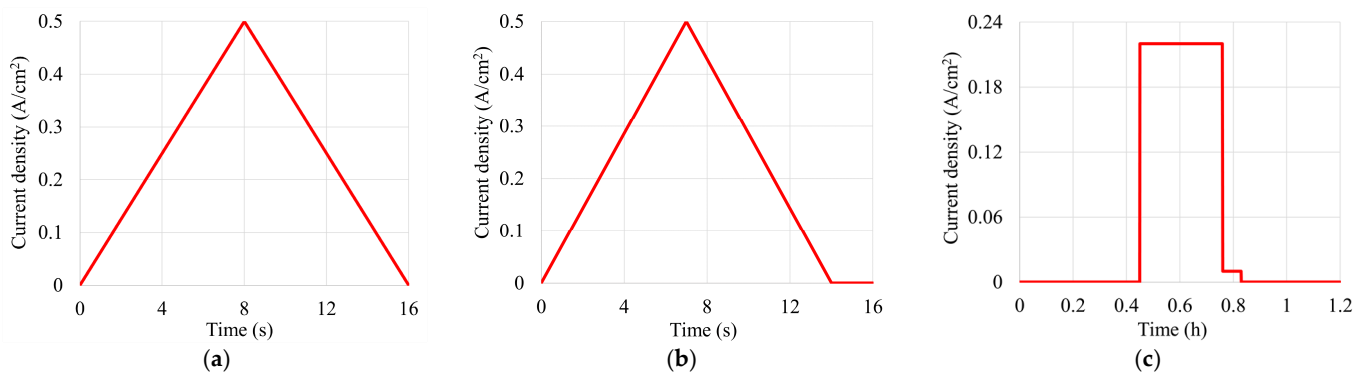
Figure 2. Load profiles: (**a**) triangular sweep cycles, (**b**) triangular sweep cycles with 2 s permanence at OCV and (**c**) Start and Stop cycles.

The cell performance degradation was measured by recording polarization curves (PC), together with electrochemical impedance spectroscopy (EIS) and cyclic voltammetry (CV). Polarization curves were carried out following a specific procedure based on the European Commission Joint Research Centre (JRC) recommendations [22,23]. In particular, reactants flows were kept constant over the entire polarization curve as suggested for single cell testing in [23]. Hydrogen and air flowrates were set to 0.5 and 2.0 sl/min, respectively. For each point of the PCs, a steady state condition was maintained for two minutes. The galvanostatic mode was set to measure the polarization curves from 0 to 500 mA/cm^2 with steps of 22 mA/cm^2. EIS was conducted according to the methodology described in [24]. The EISs were carried out in galvanostatic mode at three different current density levels: 22, 220 and 330 mA/cm^2. The amplitude of the perturbation sinusoidal function was chosen to be of 10% of the base current. The EIS spectrum was measured for 100 frequencies from 0.1 Hz to 1000 Hz. The CVs were carried out with a constant hydrogen flow of 0.4 sl/min at the anode side and a constant nitrogen flow of 0.5 sl/min at the cathode side by following the methodology already used in a previous work by the authors [11]. The minimum and maximum applied voltages were 0.03 and 0.60 V, with a scan rate of 0.2 mV/s. Finally, the electrochemical surface area (ECSA) was calculated from the hydrogen desorption peak of the CV with Equation (1) applying the methodology suggested in [25]:

$$\text{ECSA} = \frac{q_{Pt}}{\Gamma \cdot L} \left(cm^2_{Pt}/g_{Pt} \right), \tag{1}$$

where q_{Pt} is the charge density obtained from the CV experiment in C/cm$^2_{electrode}$, Γ is the charge required to reduce a monolayer of protons on Pt equal to 210 µC/cm$^2_{Pt}$, and L is the Pt content or loading in the electrode g$_{Pt}$/cm$^2_{electrode}$. Afterwards, all MEAs were analysed with SAXS technique to determine the nano-morphological modifications of the MEAs.

2.1. Small Angle X-ray Scattering (SAXS) Analysis

At the end of the load cycles all MEAs were subjected to SAXS analysis according to the methodology already adopted by the authors in a previous work [3]. SAXS is a standard technique to characterize the structure of colloidal systems. The elastic scattering of X-rays caused by the electron density inhomogeneity within the sample is exploited by this technique. Size, shape, and distribution of colloids are the information that can be obtained with this type of analysis.

2.1.1. Beamline Setup

The experiments were carried out at the Austrian SAXS beamline of the synchrotron radiation source Elettra-Sincrotrone Trieste, Italy [26]. The beamline was set to have a beam dimension of about 1.0 mm $\times$ 0.5 mm, sample to detector distance of 80 cm and an X-ray wavelength λ of 1.54 Å. The SAXS images were collected using a 2D detector (Pilatus 1M, Dectris Ltd., Baden-Daettwil, Switzerland) with a typical exposure time of 3 s. To calibrate the angular scale of the detector, silver behenate was used [27]. All the images obtained by the detector were then averaged over the azimuthal angle. This was carried out by employing the software FIT2D to achieve a 1D scattering pattern in regards to the scattering vector $q = 4\pi \sin\theta / \lambda$ (where θ is the half-value of the scattering angle, λ is the X-ray wavelength) [28] The final q-range was from 0.1 to 4.0 nm^{-1}. All integrated scattering curves were normalized with respect to the primary beam intensity. The intensity value was as well corrected on the base of the transmitted beam intensity measured by a photodiode in the beam stop. The air scattering has then been subtracted from each scattering pattern.

2.1.2. Fitting of the Intensity Curves

A polydispersed system of spherical adhesive particles is considered by the model simulating the catalyst layer NPs. The model accounts for particles with a narrow and deep attractive inter-particle potential [29]. Moreover, a log-normal volume distribution of the particle sizes is assumed. The volume size distribution was selected to improve the stability of the fitting. The contribution of the carbon present in the gas diffusion layer (GDL) and the catalyst layer of the MEAs was modelled with a power law, based on the idea of the Porod law [27]. Different parameters such as the mean radius of the particles R, and the root mean square deviation of the radius σ_R of the log-normal particle size distribution are implemented in the model. Moreover, the volume fraction of the particles surrounding every single particle v_f is included in the model. Finally, the inter-particle potential square-well width λ, and depth ε are other two critical parameters of the model. These parameters were determined by a non-linear weighted least square fitting of the model to the experimental curve with the program IGOR Pro (Wavemetrics, Lake Oswego, OR, USA) [3].

3. Results

In this section, the results achieved by applying the methods and techniques above-mentioned are reported. In particular, the outcomes of the polarization curve (PCs), electrochemical impedance spectroscopy (EIS) and cyclic voltammetry (CV) experiments are presented, together with the SAXS measurements.

3.1. Polarization Curves

Polarization curves were recorded following the methodology described in Section 2. Figure 3 depicts the polarization curves at the beginning and at the end of the aging tests. Figure 3 refers to (a) MEA CL_1, (b) MEA SS_2, (c) MEA OCV_1, and (d) MEA OCV_2 operated at constant load (440 h), start and stop (300 cycles), OCV (126 h) and OCV (400 h), respectively. Comparing initial performances of the four MEAs it is noticeable that even if they are exactly of the same type, their initial performance differs substantially. This is

attributable to fabrication differences due to the low scale production of this type of MEAs that indicates the production procedure remains quite artisanal.
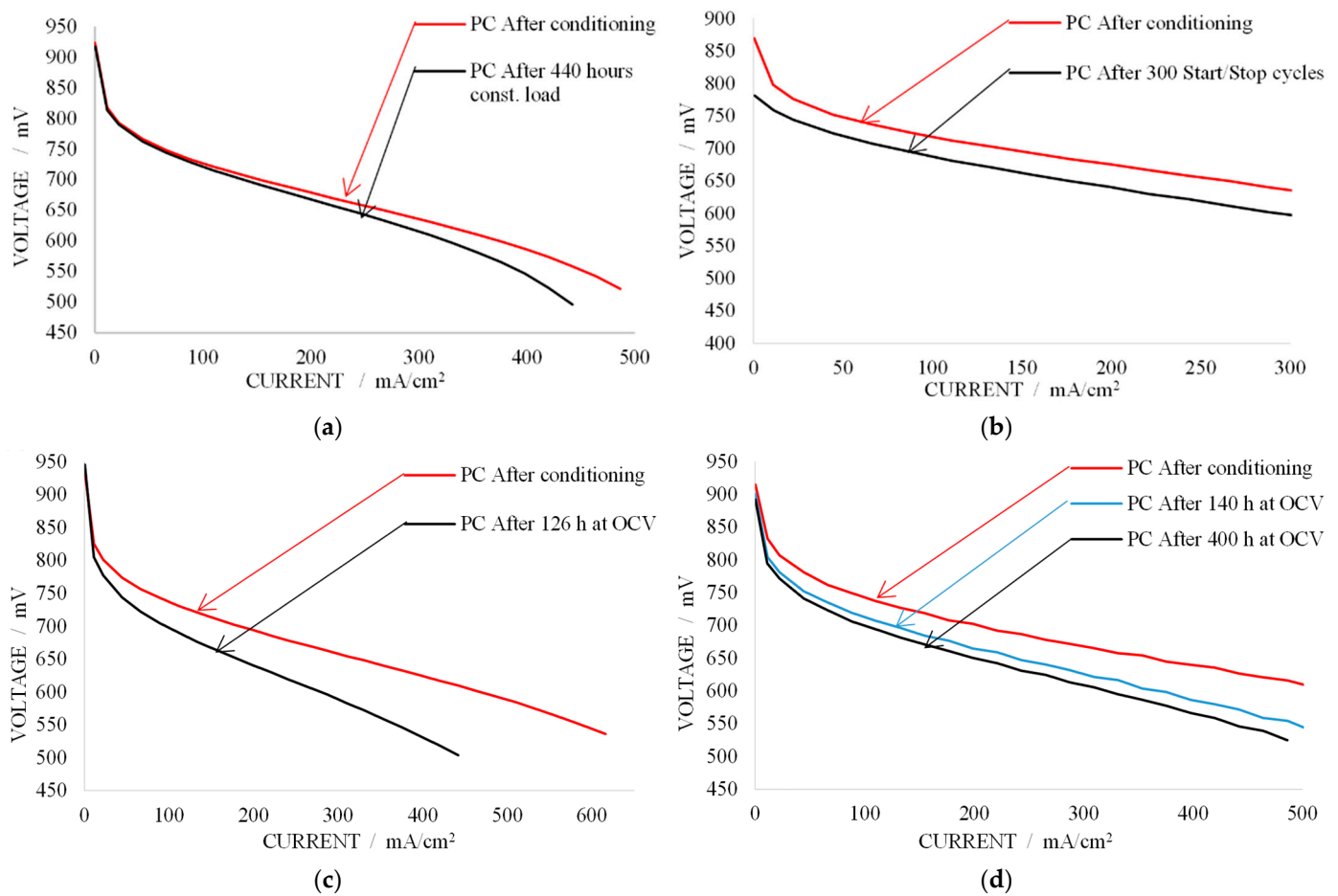
Figure 3. Polarization curves (PCs) of (**a**) MEA CL_1, (**b**) MEA SS_2, (**c**) MEA OCV_1, (**d**) MEA OCV_2.

The degradation rate for constant load operation of MEA CL_1 (Figure 3a) was found to be 30 μV/h at 0.22 mA/cm^2 and 140 μV/h at 450 mA/cm^2 which is in good agreement with data reported in [30,31] for similar PBI MEAs. For MEA CL_2 operated at constant load a degradation value of 29 μV/h was found as already reported by the authors in [11]. As a comparison, a homemade PBI MEA was tested for 780 h of constant load at 0.2 A/cm^2 in [30], and a degradation rate of 25 μV/h was reported. Instead, a 500 h test was carried out at constant load operation of 0.64 A/cm^2 in [31] and a degradation rate of 150 μV/h was observed. In [32], a degradation rate of 33 μV/h at 0.2 mA/cm^2 was measured for a 1000 h test at constant load of 0.2 mA/cm^2. Finally, a degradation rates of 5 μV/h was reported for Celtec P-1000 MEAs operated at constant load in a 6000 h test [33]. Total duration of the test could influence hourly degradation, since stronger degradation seems to occur at the beginning of the test.

MEA SS_2 was subjected to 300 start-stop cycles. The degradation rate at 0.22 mA/cm^2 of MEA SS_2 was 81 μV/h. It is noticeable from Figure 3b that this operation condition strongly affects the OCV value, probably due to membrane failure as better described in Section 4. In a previous work [3], the authors performed a 1000 start-stop cycles test and found a degradation rate of 55 μV/h. Also in this case, it might be speculated that the duration of test could influence the degradation rate value. Schmidt and Baurmeister [33] performed a 6000 h test (340 start-stop cycles) on Celtec-P1000 MEAs operated at 160 °C and reported a degradation rate of 11 μV/h at 0.2 mA/cm^2, while a degradation rate of

170 μV/h for the same MEAs operated in start-stop mode at 150 °C for 480 h (20 start-stop cycles) was reported in [34].

　　As described in [12], high potentials are responsible of the degradation of the catalyst and its support. The PC analysis of MEA OCV_1 shows high total performance degradation at high current level, but almost no degradation in terms of OCV value (see Figure 3c). The degradation rate at 0.22 mA/cm^2 for MEA OCV_1 was found to be 444 μV/h after the 126 h test. As a comparison, a 350 h test was carried out on similar PBI MEAs operated at OCV at 180 °C in [15]. An initial degradation rate of 2285 μV/h at 0.2 mA/cm^2 during the first 17 h of test was estimated from the polarization curves published in the paper. On the other hand, the overall degradation during the 350 h was assessed to be 408 μV/h at 0.2 mA/cm^2. This behavior was encountered also in this study when analyzing the results for MEA OCV_2. This latter was operated for 400 h at OCV, and a total degradation rate of 124 μV/h was found over the 400 h of test at 0.22 mA/cm^2 (see Figure 3d). Instead, a degradation rate of 659 μV/h was measured after the first 140 h of operation. The estimated reduction of ECSA after the aging tests for some of the MEAs is reported in Table 2, while Table 3 shows the degradation rates of all the MEAs tested by the authors allowing a comparison of the load profile influence on fuel cell performance degradation.

Table 2. ECSA reduction estimated with cyclic voltammetry at the beginning and at the end of the aging test.

MEA Label	ECSA Reduction
MEA TRG	-
MEA TRG_OCV_1	-
MEA TRG_OCV_2	50%
MEA CL_1	30%
MEA CL_2	30%
MEA SS_1	-
MEA SS_2	-
MEA OCV_1	10%
MEA OCV_2	10%

Table 3. Degradation rate values and mean catalyst Pt particles radii of tested MEAs obtained with the SAXS analysis.

MEA Label	Pt Particles Size (nm)		Degradation Rate
	r_{mean}	St. dev.	(μV/h)
MEA Ref_1—previous work [3]	2.78	0.64	-
MEA Ref_2	2.38	0.59	-
MEA TRG—previous work [3]	4.88	0.66	34
MEA TRG_OCV_1—previous work [3]	5.60	0.66	45
MEA TRG_OCV_2	5.51	0.76	44
MEA CL_1	4.65	0.70	30
MEA CL_2	4.41	0.72	29
MEA SS_1	5.02	0.65	55
MEA SS_2	4.71	0.53	81
MEA OCV_1	3.82	0.66	444
MEA OCV_2	3.98	0.69	124

3.2. Electrochemical Impedance Spectroscopy (EIS)

In Figure 4, the EIS results of MEA SS_2, MEA OCV_1 and MEA OCV_2 at 22 mA/cm^2, 220 mA/cm^2 and 330 mA/cm^2 before and after aging tests are presented.
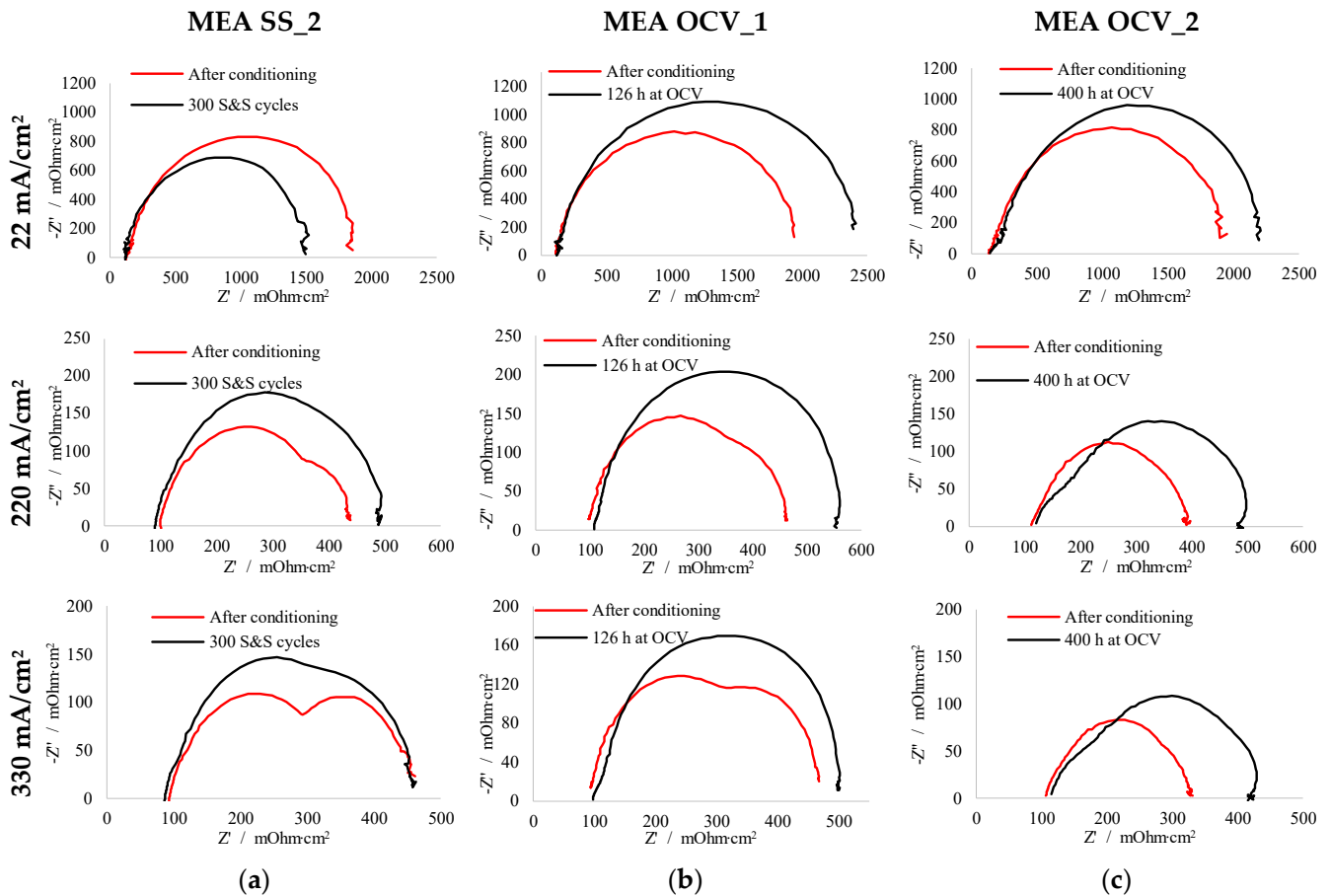
Figure 4. EIS spectrum at 22 mA/cm^2, 220 mA/cm^2 and 330 A/cm^2 of (**a**) MEA SS_2, (**b**) MEA OCV_1, (**c**) MEA OCV_2.

The EIS spectrum for PEM fuel cells can be divided in three zones [35]. At high frequencies, the intercept with the *x*-axis represents the Ohmic electrolyte losses, and the first high frequencies arc (not visible in these experimental results) represents the anode activation losses. Instead, the second arc represents the cathode activation losses, while the last low frequencies arc indicates the mass transport effects. It must be noticed that a reduction of polarization (EIS spectrum arc dimension) during the aging test is observable for MEA SS_2 at low current (see Figure 4a at 22 mA/cm^2). This type of aging test influenced the EIS spectra at low current indicating that probably the nature and morphology of the electrode/electrolyte interface has changed. It is remarkable that for high current densities the evolution of the spectra brings to an increasing of the polarization, while at low current the polarization decreased during the aging test. This phenomenon was already encountered by Seo et al. [36] and explained as a result of water-back diffusion which increases the conductivity in the ionomer. In [37], a reduction of the EIS spectra for LTPEM fuel cells subjected to on-off cycles with a humidity of less than 10% was observed as well, while the polarization increased with time during the aging test in presence of high humidity. the impact of humidification on charge transfer for HTPEM is well known even though has a lower effect compared to LTPEM. This could justify the EIS spectra evolution of MEA SS_2 at low current densities.

On the other hand, the polarization arc increasing along the aging of the MEAs OCV_1 and OCV_2 occurs at all current densities (see Figure 4b,c) in accordance with data obtained

in [15] where similar MEAs were subjected to 244 h of OCV permanence. It is noticeable that the reduction of the polarization with the increasing of the current density is more evident in MEA OCV_2 than in MEA OCV_1, and polarization is lower for MEA OCV_2 despite its longer permanence at OCV. In MEA OCV_2 an increase of the 45° linear branch at high frequency is also visible [24].

3.3. Cyclic Voltammetry (CV)

Cyclic Voltammetry was executed at the beginning and at the end of the aging test, with the purpose to establish the order of magnitude of ECSA reduction following the methodology already used by the authors [11] and described in Section 2. It has been assumed that the estimation of the ECSA reduction directly derives from the CV measurement outcomes and are strictly correlated. For this reason, only the ECSA reduction values are reported in this section. The ECSA reduction values for each tested MEA are reported in Table 2. In particular, the values for the MEAs TRG_OCV_2, CL_1, CL_2, OCV_1 and OCV_2 are collected. It can be noticed that the largest reduction was obtained for MEA TRG_OCV_2. Surprisingly, the smallest ECSA reduction was estimated for MEA OCV_1 and 2 even though the degradation rates were the highest for these MEAs. Finally, it was not possible to estimate the ECSA reduction value of MEA SS 1 and 2 due to membrane failure after the aging tests.

3.4. Small Angle X-ray Scattering (SAXS) Measurements

In Table 3, the values of the Pt catalyst mean radius obtained with SAXS techniques are reported.

Figure 5a shows the comparison between the two log-normal volume distributions obtained by the SAXS analysis results of the two MEAs: MEA Ref_1 and MEA Ref_2. The MEAs Ref_1 and Ref_2 are the reference ones which were not subjected to any aging tests. In this study, a first Pt mean radius measurement was performed on the untouched MEA Ref_2, and the obtained data were compared with the ones obtained for MEA Ref_1 in previous SAXS analysis [3] with the purpose to verify the repeatability and reproducibility of the measurement as well as the uniformity of manufacturing of the MEAs. The Pt mean radius values of these two MEAs are 2.61 nm for MEA Ref_1 and 2.38 nm for MEA Ref_2.

Figure 5b shows the log-normal volume distributions obtained for MEAs TRG, TRG_OCV_1, and TRG_OCV_2. The MEA Ref_1 has been used as reference MEA. These MEAs, except for MEA TRG_OCV_2, had already been tested and analyzed in a previous work [3]. The Pt mean radius values at the end of the load cycling test for MEA TRG, TRG_OCV_1 and TRG_OCV_2 was found to be 4.88, 5.60 and 5.51 nm respectively. MEA TRG_OCV_1 and MEA TRG_OCV_2 were operated with the same load cycle profile (0–0.5 V, 2 s OCV), while MEA TRG was subjected to a triangular load cycle profile between 0.01–0.5 V. For MEA TRG_OCV_1 and MEA TRG_OCV_2 the difference of the Pt mean radius values is 0.11 nm (almost 2%). While MEA TRG Pt mean radius is sensitively smaller: around 13% with respect to TGR_OCV_1 and 11% with respect to TGR_OCV_2.

In Figure 5c MEA Ref_2 is used as reference. Here, the distributions of the MEA SS_1 and SS_2 that were subjected to 1000 and 300 Start and Stop cycles, respectively, are reported. The SAXS analysis of MEA SS_2 showed that the Pt mean radius at the end of the test was 4.71 nm while for MEA SS_1 the Pt mean radius at the end of the test was 5.02 nm. It can be noticed that the lower number of Start and Stop cycles performed on MEA SS_2 with respect to SS_1 had the double effect of slightly lowering the mean radius of the Pt particles, as expected, but also lowering the spreading of the distribution due to degradation.
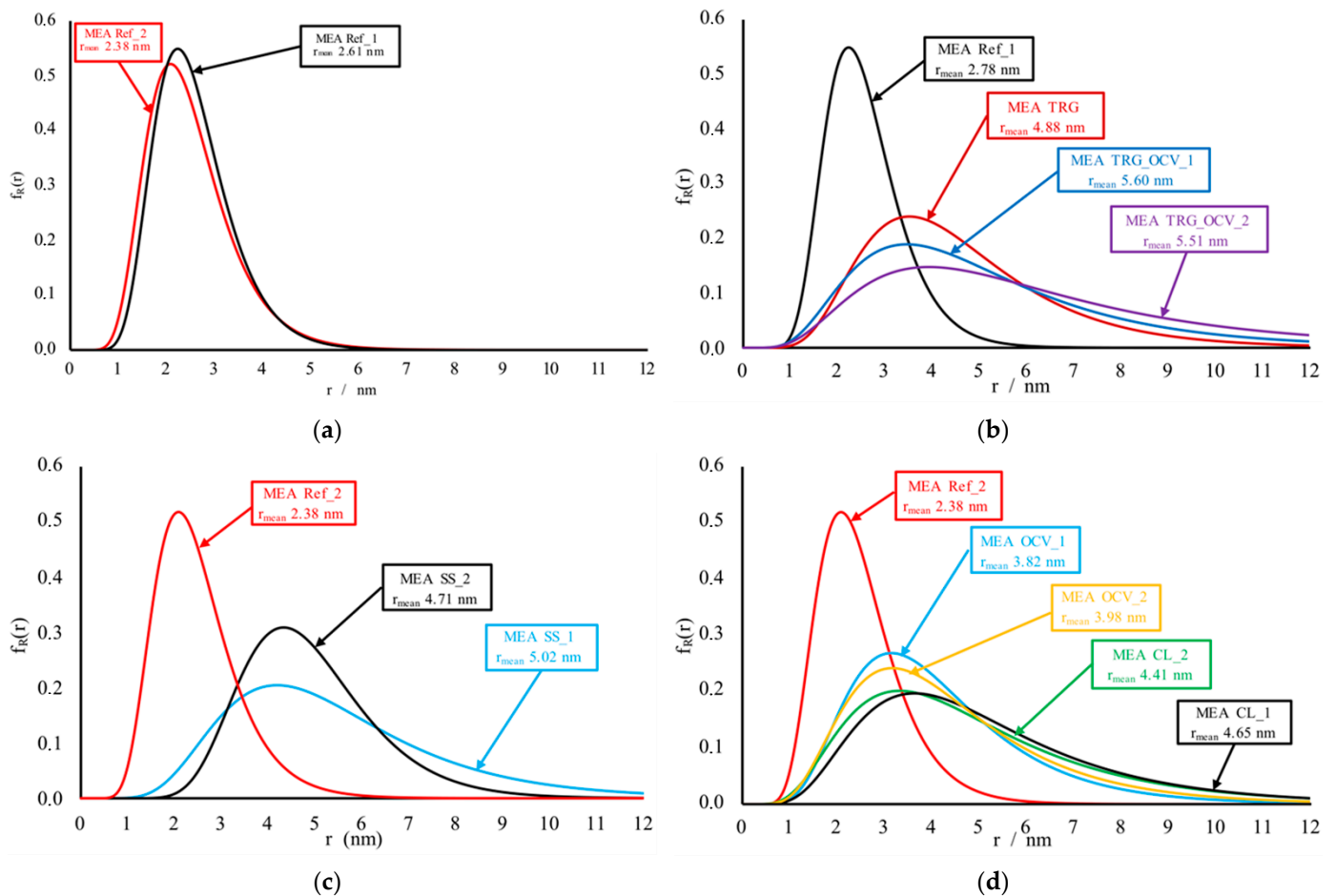
Figure 5. Pt nanoparticles size distribution. (**a**) MEA Ref_1 (black line) and Ref_2 (red line), (**b**) MEA Ref_1 (black line), TRG (red line), TRG_OCV_1 (grey line) and TRG_OCV_2 (purple line), (**c**) MEA Ref_2 (red line), SS_2 (black line), SS_1 (blue line), (**d**) MEA Ref_2 (red line), OCV_1 (blue line) and OCV_2 (yellow line), CL_2 (green line) and CL_1 (black line).

In Figure 5d the MEA Ref_2 was used as reference MEA. The two MEAs subjected to constant load have a similar Pt mean radius value as expected. These values are 4.65 and 4.41 nm for MEA CL_1 and CL_2, respectively. As already highlighted in Section 3.1, also the degradation rate of these two MEAs is similar. The MEA OCV_1 was subjected to OCV. This MEA has a degradation rate that is almost 10 times higher than the other MEAs, but his Pt mean radius at the end of the test was 3.82 nm which is the lowest Pt mean radius value, except for the reference MEAs.

4. Discussion

As described in Section 3.1, high potentials are responsible of the degradation of the catalyst and its support. Polarization curve analysis of MEA OCV_1 shows high total performance degradation at high current level, but almost no degradation in terms of OCV value. This could be explained attributing the performance degradation to the carbon support corrosion with a consequent increasing of mass transport losses and an increasing of cathode activation losses. The hydrophilicity of the carbon surface is enhanced by the carbon corrosion/oxidation [38]. This phenomenon can provoke H_3PO_4 flooding on the carbon surface, hence a higher mass transport resistance is generated [15]. As highlighted in Section 3.2, EIS do not allow clear distinction between cathode activation losses increasing and mass transport limitation phenomena. However, since SAXS showed a limited platinum particle agglomeration (see Section 3.4), it can be inferred that for MEA OCV_1 and MEA OCV_2 the dominant degradation effect could be the carbon

support corrosion with consequent phosphoric acid flooding and eventually depletion as explained in [39].

In the literature, the OCV operation is often cited as one of the main causes of platinum agglomeration [15]. However, the process of platinum agglomeration is a complex phenomenon that occurs through other intermediate steps: firstly, carbon corrosion happens, favored by high potentials. Secondly, carbon corrosion causes the augmentation of hydrophilicity of the carbon support which causes phosphoric acid flooding which can be at the origin of platinum depletion and agglomeration. For MEA OCV_1 and MEA OCV_2 the platinum agglomeration does not seem to be the major cause of degradation. For MEA OCV_1, it could be possible that platinum did not have enough time to agglomerate since it was operated for a relatively short time. A slight reduction of OCV voltage after 400 h of test is visible in the polarization curves by analyzing the degradation data of MEA OCV_2, and a higher ECSA reduction in comparison with MEA OCV_1 is observed. This may indicate that Pt agglomeration actually played a role in this case. However, EIS data showed that phosphoric acid depletion might also have an important role on the ECSA reduction. Finally, SAXS results suggest that the major role in the degradation due to OCV operation should be attributed to acid leaching effects even if a higher agglomeration of platinum occurred for MEA OCV_2.

Analyzing the EIS results, the reduction of the polarization with the increasing of the current indicates that the MEA internal losses are mainly affected by charge transfer resistance. For MEA OCV_1, the dependence of the EIS spectra with the current seems to be lower than for MEA OCV_2. Therefore, it may be speculated that the mass transport loss contributes more to the polarization of the EIS spectrum in MEA OCV_1 than in MEA OCV_2. Catalyst agglomeration, carbon corrosion and acid loss from the electrodes are three different degradation mechanisms that may increase the charge transfer resistance. As reported in [40], a lower acid content in the cathode catalyst layer increases the proton transport resistance of the electrodes. In the EIS spectra, this effect becomes evident with the increase of the 45° linear branch at high frequency [24] which is quite evident in the EIS spectra of MEA OCV_2 at high current densities. This could indicate that, in MEA OCV_1, the polarization of the EIS spectra increase is due to a combined effect: on one hand the charge transfer resistance increases due to carbon corrosion while on the other hand the mass transport resistance grows due to phosphoric acid flooding of the carbon pores. For MEA OCV_2, it might be conjectured that the depletion of acid caused a reduction of the ECSA, but mass transport resistance is less important since there is less or no flooding effect. This could explain the reduced total EIS spectra of MEA OCV_2 with respect to MEA OCV_1 in spite of the higher ECSA loss for MEA OCV_2 with respect to MEA OCV_1.

Differently from the other operational conditions, start and stop cycles seem to affect the OCV value. This could be attributed to reactant cross-over due to membrane thinning and creation of pinholes and/or reduction of ECSA, caused by platinum agglomeration. The cross-over current could be measured by means of linear sweep voltammetry (LSV) technique as carried out by Rastedt et al. [41] to experimentally verified the supposed membrane thinning phenomenon. The loss in OCV value during start and stop cycles has been reported be many authors and membrane degradation is usually considered the main degradation factor [42] together with a loss in ECSA [43]. Analyzing the EIS spectra, it is noticeable that aging test influences the EIS spectra also at low currents indicating that the nature and morphology of the electrode/electrolyte interface has probably changed. In particular, it is remarkable that for high current densities the evolution of the spectra brings to an increasing of the polarization, while at low current the polarization actually decreased during the aging test. It is interesting to notice that membrane failure had also be encountered on MEA SS_1 subjected to the same start and stop cycle during a previous test performed by the research group of the University of Trieste. This allows us to infer that start and stop cycles are an important stressor for membrane structure degradation. Analyzing the SAXS results for MEA SS_1 and MEA SS_2, it is noticeable that the two distributions follows the same behavior during the start and stop aging test that seems

to cause a displacement toward right in the direction of higher radii values in a most noticeable manner with respect to other operating conditions, as shown in Figure 5b,c. This means that start and stop cycles cause a higher increase of the mode radius value than the mean radius increase, which could suggest that degradation due to start and stop cycles causes a more generalized and uniform particle size growing over the entire MEA surface compared to other operational conditions.

5. Conclusions

In this paper, the effect of the operating conditions on a HT-PEM fuel cells are experimentally analyzed. In particular, the effects of open circuit voltage (OCV) and start-stop cycles were studied with electrochemical diagnostic tools such as polarization curves, EIS and CV. Degradation results were compared with previous experimental data collected by the authors in other works. It was shown that OCV condition, start and stop cycling and load cycling increase degradation of the MEAs compared to constant load operation, and that OCV is the operational condition that enhances degradation the most.

In order to provide more information on the degradation phenomena, the catalyst nano-morphology evolution was also assessed using ex situ SAXS analysis to support the interpretation of EIS and CV results. To the authors' knowledge, the SAXS technique was used to analyze HTPEM MEA constantly subjected to OCV for the first time. SAXS analysis allows to suggest Pt agglomeration as the main cause of degradation for MEAs subjected to load cycling while for OCV operation, even if for long term operation its effect on Pt agglomeration is widely recognized, in this work carbon corrosion and acid depletion were suggested to be the two dominant degradation mechanisms. Concerning start and stop cycles, the main degradation phenomenon was identified in membrane related degradation processes, in particular, the creation of pinholes with consequent reactants cross-over. This was the cause of membrane failure and the impossibility to perform the ECSA reduction determination.

This study provides additional experimental data on the behavior of HTPEM MEA subjected to different operational profiles with the aim to cover the knowledge gap on degradation mechanisms still present in literature. In fact, a large number of data and experiments must be available to increase the statistical contribution. Moreover, the operating profiles employed in this study may be part of a standardized testing protocol for HTPEM MEAs. Finally, it is suggested to reproduce the presented aging tests to verify the outcomes of this study and employ different techniques such as in situ SAXS or transmission electron microscopy (TEM) to analyze the agglomeration of Pt particles in future studies.

Conflicts of Interest: The authors declare no conflict of interest.

References

1. Taccani, R.; Ustolin, F.; Zuliani, N.; Pinamonti, P.; Pietra, A. Fuel Cells and Shipping Emissions Mitigation. In *Technology and Science for the Ships of the Future: Proceedings of NAV 2018: 19th International Conference on Ship and Maritime Research*; IOS Press: Amsterdam, The Netherlands, 2018; pp. 885–892.
2. Ustolin, F.; Taccani, R. Fuel Cells for Airborne Usage: Energy Storage Comparison. *Int. J. Hydrogen Energy* **2018**, *43*, 11853–11861. [CrossRef]
3. Valle, F.; Zuliani, N.; Marmiroli, B.; Amenitsch, H.; Taccani, R. SAXS Analysis of Catalyst Degradation in High Temperature PEM Fuel Cells Subjected to Accelerated Ageing Tests. *Fuel Cells* **2014**, *14*, 938–944. [CrossRef]
4. Moçotéguy, P.; Ludwig, B.; Scholta, J.; Barrera, R.; Ginocchio, S. Long Term Testing in Continuous Mode of HT-PEMFC Based H3PO 4/PBI Celtec-PMEAs for μ-CHP Applications. *Fuel Cells* **2009**, *9*, 325–348. [CrossRef]

5. Oono, Y.; Sounai, A.; Hori, M. Long-Term Cell Degradation Mechanism in High-Temperature Proton Exchange Membrane Fuel Cells. *J. Power Sources* **2012**, *210*, 366–373. [CrossRef]

6. Oono, Y.; Sounai, A.; Hori, M. Prolongation of Lifetime of High Temperature Proton Exchange Membrane Fuel Cells. *J. Power Sources* **2013**, *241*, 87–93. [CrossRef]

7. Voorhees, P.W. Ostwald Ripening of Two-Phase Mixtures. *Annu. Rev. Mater. Sci.* **1992**, *22*, 197–215. [CrossRef]

8. Takajo, S. Analysis of Particle Growth by Coalescence during Liquid Phase Sintering. *Acta Met.* **1984**, *32*, 107. [CrossRef]

9. Kerr, R.; García, H.R.; Rastedt, M.; Wagner, P.; Alfaro, S.M.; Romero, M.T.; Terkelsen, C.; Steenberg, T.; Hjuler, H.A. Lifetime and Degradation of High Temperature PEM Membrane Electrode Assemblies. *Int. J. Hydrogen Energy* **2015**, *40*, 16860–16866. [CrossRef]

10. Smith, M.C.; Gilbert, J.A.; Mawdsley, J.R.; Seifert, S.; Myers, D.J. In Situ Small-Angle X-Ray Scattering Observation of Pt Catalyst Particle Growth during Potential Cycling. *J. Am. Chem. Soc.* **2008**, *130*, 8112–8113. [CrossRef]

11. Taccani, R.; Chinese, T.; Boaro, M. Effect of Accelerated Ageing Tests on PBI HTPEM Fuel Cells Performance Degradation. *Int. J. Hydrogen Energy* **2017**, *42*, 1875–1883. [CrossRef]

12. Büchi, N.; Inaba, M.; Schmidt , J. *Polymer Electrolyte Fuel Cell Durability*; Springer: New York, NY, USA, 2009.

13. Liu, S.; Rasinski, M.; Lin, Y.; Wippermann, K.; Everwand, A.; Lehnert, W. Effects of Constant Load Operations on Platinum Bands Formation and Cathode Degradation in High-Temperature Polymer Electrolyte Fuel Cells. *Electrochim. Acta* **2018**, *289*, 354–362. [CrossRef]

14. Zhang, J. *PEM Fuel Cell Electrocatalysts and Catalyst Layers*; Springer: London, UK, 2008.

15. Qi, Z.; Buelte, S. Effect of Open Circuit Voltage on Performance and Degradation of High Temperature PBI-H3PO4fuel Cells. *J. Power Sources* **2006**, *161*, 1126–1132. [CrossRef]

16. Wu, J.; Yuan, X.Z.; Martin, J.J.; Wang, H.; Zhang, J.; Shen, J.; Wu, S.; Merida, W. A Review of PEM Fuel Cell Durability: Degradation Mechanisms and Mitigation Strategies. *J. Power Sources* **2008**, *184*, 104–119. [CrossRef]

17. Zhang, S.; Yuan, X.Z.; Hin, J.N.C.; Wang, H.; Wu, J.; Friedrich, K.A.; Schulze, M. Effects of Open-Circuit Operation on Membrane and Catalyst Layer Degradation in Proton Exchange Membrane Fuel Cells. *J. Power Sources* **2010**, *195*, 1142–1148. [CrossRef]

18. Haubold, H.G.; Wang, X.H.; Jungbluth, H.; Goerigk, G.; Schilling, W. In situ anomalous small-angle X-ray scattering and X-ray absorption near-edge structure investigation of catalyst structures and reaction. *J. Mol. Struct.* **1996**, *383*, 283–289. [CrossRef]

19. Stevens, D.A.; Zhang, S.; Chen, Z.; Dahn, J.R. On the determination of platinum particle size in carbon-supported platinum electrocatalysts for fuel cell applications. *Carbon* **2003**, *41*, 2769–2777. [CrossRef]

20. Yu, C.; Holby, E.F.; Yang, R.; Toney, M.F.; Morgan, D.; Strasser, P. Growth Trajectories and Coarsening Mechanisms of Metal Nanoparticle Electrocatalysts. *ChemCatChem* **2012**, *4*, 766–770. [CrossRef]

21. Gilbert, J.A.; Kropf, A.J.; Kariuki, N.N.; DeCrane, S.; Wang, X.; Rasouli, S.; Yu, K.; Ferreira, P.J.; Morgan, D.; Myers, D.J. In-Operando Anomalous Small-Angle X-Ray Scattering Investigation of Pt 3 Co Catalyst Degradation in Aqueous and Fuel Cell Environments. *J. Electrochem. Soc.* **2015**, *162*, F1487–F1497. [CrossRef]

22. Kabza, A.; Malkow, T.; Antoni, L.; Muñoz, M.; Tsotridis, G.; Pilenga, A.; Schätzle, M.; Rosini, S.; Van Bogaert, G.; Thalau, O.; et al. *PEFC Power Stack Performance Testing Procedure. Measuring Voltage and Power as Function of Current Density. Polarisation Curve Test Method*; Test module PEFC ST 5-3; JRC European Commission: Petten, The Netherlands, 2009.

23. De Marco, G.; Pilenga, A.; Honselaar, M.; Malkow, T.; Tsotridis, G.; Janssen, A.; Rietveld, B.; Vinke, I.; Kiviaho, J. *Testing the Voltage and Power as Function of Current Density. Polarisation Curve for a SOFC Single Cell*; Test Module TM SOFC M01; JRC European Commission: Petten, The Netherlands, 2010.

24. Galbiati, S.; Baricci, A.; Casalegno, A.; Marchesi, R. Degradation in Phosphoric Acid Doped Polymer Fuel Cells: A 6000 h Parametric Investigation. *Int. J. Hydrogen Energy* **2013**, *38*, 6469–6480. [CrossRef]

25. Cooper, K.R. In Situ Pem Fuel Cell Electrochemical Surface Area and Catalyst Utilization Measurement. Available online: https://www.scribner.com/wp-content/uploads/2017/06/Scribner-on-ECSA-Fuel-Cell-Magazine-2009.pdf (accessed on 14 October 2021).

26. Amenitsch, H.; Bernstorff, S.; Kriechbaum, M.; Lombardo, D.; Mio, H.; Rappolt, M.; Laggner, P. Performance and First Results of the ELETTRA High-Flux Beamline for Small-Angle X-ray Scattering. *J. Appl. Crystallogr.* **1997**, *30*, 872–876. [CrossRef]

27. Huang, T.C.; Toraya, H.; Blanton, T.N.; Wu, Y. X-Ray Powder Diffraction Analysis of Silver Behenate, a Possible Low-Angle Diffraction Standard. *J. Appl. Crystallogr.* **1993**, *26 Pt 2*, 180–184. [CrossRef]

28. Hammersley, A.P. *ESRF Internal Report, ESRF98HA01T, FIT2D V9.129 Reference Manual V3.1*; European Synchrotron Radiation Facility: Grenoble, France, 1998.

29. Pontoni, D.; Finet, S.; Narayanan, T.; Rennie, A.R. Interactions and Kinetic Arrest in an Adhesive Hard-Sphere Colloidal System. *J. Chem. Phys.* **2003**, *119*, 6157–6165. [CrossRef]

30. Modestov, A.D.; Tarasevich, M.R.; Filimonov, V.Y.; Zagudaeva, N.M. Degradation of High Temperature MEA with PBI-H 3 PO 4 Membrane in a Life Test. *Electrochim. Acta* **2009**, *54*, 7121–7127. [CrossRef]

31. Hu, J.; Zhang, H.; Zhai, Y.; Liu, G.; Yi, B. 500 h Continuous Aging Life Test on PBI/H3PO4 High-Temperature PEMFC. *Int. J. Hydrogen Energy* **2006**, *31*, 1855–1862. [CrossRef]

32. Bandlamudi, G. *Systematic Characterization of HT PEMFCs Containing Pbi/H3PO4 Systems. Thermodynamic Analysis and Experimental Investigations*; Logos Verlag Berlin GmbH: Berlin, Germany, 2011.

33. Schmidt, T.J.; Baurmeister, J. Properties of high-temperature PEFC Celtec®-P 1000 MEAs in start/stop operation mode. *J. Power Sources* **2008**, *176*, 428–434.

34. Kim, J.; Kim, M.; Lee, B.G.; Sohn, Y.J. Durability of High Temperature Polymer Electrolyte Membrane Fuel Cells in Daily Based Start/Stop Operation Mode Using Reformed Gas. *Int. J. Hydrogen Energy* **2015**, *40*, 7769–7776. [CrossRef]

35. O'Hayre, R.; Cha, S.-W.; Colella, W.; Prinz, F.B. *Fuel Cell Fundamentals*; John Wiley & Sons: Hoboken, NJ, USA, 2006.

36. Arif, A.; Devianto, H.; Isdiriayani, N. EAP13-4571 PEMFC Carbon Corrosion Due to Start-Stop Cycling. In Proceedings of the NACE East Asia Pacific Rim Conference, Kyoto, Japan, 19–21 November 2013.

37. Seo, D.; Lee, J.; Park, S.; Rhee, J.; Won, S.; Shul, Y. Investigation of MEA Degradation in PEM Fuel Cell by on / off Cyclic Operation under Different Humid Conditions. *Int. J. Hydrogen Energy* **2011**, *36*, 1828–1836. [CrossRef]

38. Fairweather, J.D.; Spernjak, D.; Weber, A.Z.; Harvey, D.; Wessel, S.; Hussey, D.S.; Jacobson, D.L.; Artyushkova, K.; Mukundan, R.; Borup, R.L. *Effects of Cathode Corrosion on Through-Plane Water Transport in Proton Exchange Membrane Fuel Cells*; J. Electrochem. Soc.: Pennington, NJ, USA, 2013; Volume 160, pp. F980–F993. [CrossRef]

39. Bandlamudi, V.; Bujlo, P.; Sita, C.; Pasupathi, S. Study on Electrode Carbon Corrosion of High Temperature Proton Exchange Membrane Fuel Cell. *Mater. Today Proc.* **2018**, *5*, 10602–10610. [CrossRef]

40. Kim, J.; Yi, J.S.; Song, T. Investigation of Degradation Mechanisms of a High-Temperature Polymer-Electrolyte-Membrane Fuel Cell Stack by Electrochemical Impedance Spectroscopy. *J. Power Sources* **2012**, *220*, 54–64. [CrossRef]

41. Rastedt, M.; Pinar, F.J.; Pilinski, N.; Wagner, P. Effects of Reactant Gases on HT-PEM Fuel Cells. *ECS Trans.* **2015**, *69*, 535–549. [CrossRef]

42. Jeon, Y.; Na, H.; Hwang, H.; Park, J.; Hwang, H.; Shul, Y. Accelerated Life-Time Test Protocols for Polymer Electrolyte Membrane Fuel Cells Operated at High Temperature. *Int. J. Hydrogen Energy* **2015**, *40*, 3057–3067. [CrossRef]

43. Kannan, A.; Kabza, A.; Scholta, J. Long Term Testing of Start e Stop Cycles on High Temperature PEM Fuel Cell Stack. *J. Power Sources* **2015**, *277*, 312–316. [CrossRef]